$Al(He)_N^{3+}$ clusters: a theoretical study

Sabnam S. Ullah, Chayanika Kashyap, Ankur Kanti Guha*, Apurba Kr. Barman, Alok Ch. Kalita and Pankaz K. Sharma

Department of Chemistry, Cotton University, Panbazar, Guwahati 781 001, India

The geometries and electronic structure of molecular ions containing helium (He) atoms complexed to sodium (Na), magnesium (Mg) and aluminium (Al) cations have been studied computationally using density functional and wavefunction-based methods. The complexation of He atoms depends on the charge on the metal centre. While complexation with Na^+ and Mg^{2+} is very weak, that with Al^{3+} is found to be strong. The highest coordination number (*N*) for $AlHe_N^{3+}$ is found to be 11, which is a true minimum in the potential energy surface. Topological analysis within the realm of quantum theory of atoms in molecules reveals closed-shell interaction in these systems.

Keywords: Al–He clusters, cluster, coordination number, complexation, density functional, noble gases, wavefunction.

NOBLE gases are unreactive except under extreme conditions. Among the group members, the first noble gas, i.e. 'helium' is the most unreactive because of its high ionization energy of 577 kcal mol^{-1} (or 25 eV)[1]. Based on density functional theory and high-level *ab initio* method, Kaltsoyannis[2] predicted the formation of 17 coordinate helium–actinide complexes. This is surprising because in spite of having very high ionization energy, helium is still able to form complexes with metals. The possibility of highest coordination number for an atom is known as the generalized Gregory–Newton problem which is related to the problem of how many spheres of a given radius *R* can be packed around a unit sphere[3]. Hermann *et al.*[4] showed that the interaction of Pb^{2+} with He atoms resulted in the formation of $PbHe_{15}^{2+}$ having a Frank–Kasper polyhedron[5]. Such species with higher coordination number have been found only in liquid state[5]. In regular icosahedral structures such as rare-gas clusters and metallic clusters with $N = 12$ (where *N* is the maximum coordination number of ligands interacting with the central atom), stable structures have been reported[6]. In solid state, such as hexagonal closed packing and face-centred cubic structures, coordination number up to $N = 12$ was predicted but resulted in denser packing[7]. In binary inter-metallic alloys, coordination number 14, 15 and 16 was also found[8]. Using a genetic algorithm-based crystal structure search method together with the first-principles total energy and geometry relaxation method, Dong *et al.*[9] explained that helium forms stable solid compound with sodium (Na_2He) under high pressure. Recently Liu *et al.*[10] have shown that helium forms a stable complex with water under high pressure.

Hotokka *et al.*[11] have carried out complete active space self-consistent field (CASSCF) calculations on $AlHe^{3+}$ and reported the dissociation energy (D_0) as 27.4 kcal mol^{-1} and equilibrium bond length to be 1.67 Å. Reho *et al.*[12] measured the laser-induced fluorescence spectra of Al atoms solvated in superfluid helium nanodroplets and concluded that these atoms reside in the interior of the helium droplets. Jeff *et al.*[13] reported the first example of Al atom in the excited state becoming attached to helium nanodroplets. Supported by *ab initio* calculations, they showed that the metastable Al atom prefers to stay on the surface rather than moving to the interior. The interesting chemistry of helium with aluminium has prompted us to explore the coordination chemistry between them. We have selected Al in +3 oxidation state because most of the previous studies considered neutral Al atom[12,13] and very few studies are related to charged Al atom[11]. The selection of high oxidation state of Al is driven by the fact that Hermann *et al.*[4] have previously noted that the formation of higher coordination is expected with charged species. Moreover, to study the effect of charge on the stability of these complexes, we have also included other charged p-block metals such as Na^+ and Mg^{2+} in this study.

All the structures were fully optimized without any symmetry constraints at PBE[14], ωB97XD[15], PW91 (ref. 16) and MP2 (ref. 17) level of theory using aug-cc-pVDZ basis set. We have used dispersion-corrected functional as implemented in ωB97XD, as the interaction between the metal centre and He atom is non-covalent. Further, for comparison, we have performed the composite CBS–QB3 calculations. We have used ultrafine integration grid during optimization and the geometry convergence criteria were tightened from the default via IOP ($6/7 = 67$) which produces 10^{-4} au for the maximum force. Harmonic vibrational frequency calculations were also performed to understand the nature of the stationary states. All structures were found to be true local minimum with all real frequencies. Zero point corrections were included during incremental binding energy calculations. All geometry optimization and frequency calculations were performed using Gaussian16 suite of programs[18]. The topological analysis of electron density was done within the framework of quantum theory of atoms in molecules (QTAIM)[19] using Multiwfn program code[20].

Figure 1 shows the potential energy curves for the interaction of Al^{3+} with a single molecule of He calculated using both wavefunction-based (CCSD(T)) as well as density functional-based (PBE) methods. The system is well defined by a single reference electronic configuration as both He and Al^{3+} are closed-shell systems, and it is expected that CCSD(T) in conjunction with aug-cc-pVDZ basis set will produce good results. Both CCSD(T)

*For correspondence. (e-mail: ankurkantiguha@gmail.com)

and PBE curves are almost identical to each other with the equilibrium Al^{3+}–He distance close to 1.7 Å. A similar approach was used by Hermann *et al.*[4] for the interaction between Pb^{2+} and a single He atom.

Figure 2 shows the optimized geometries of $AlHe_N^{3+}$ with $N \leq 13$. For up to $N = 4$, conformational analysis was performed to look for the global minimum. The geometries shown in Figure 2 are global mimima for $N = 1$–4 and local minima for $N > 4$. The average Al–He distance increases with increase in N, while the average He–He distance decreases with increase in N. Table 1 shows these geometrical parameters. It is to be noted that for $N = 11$, we get a first-order saddle point which on relaxation leads to a true local minimum (Figure 2). The energy difference between the first-order saddle point and the local minimum is only 4.5 kcal mol^{-1}. The observation of a first-order saddle point for $N = 11$ prompted us to interpret that structural stability has been reached. Here 'structural stability' denotes the maximum number of He atoms that can be accommodated in the first coordination sphere of the metal ion. The observation of a first-order saddle point for $N = 11$ may indicate that this might be the highest number of He atoms that can be accommodated inside the first coordination sphere.

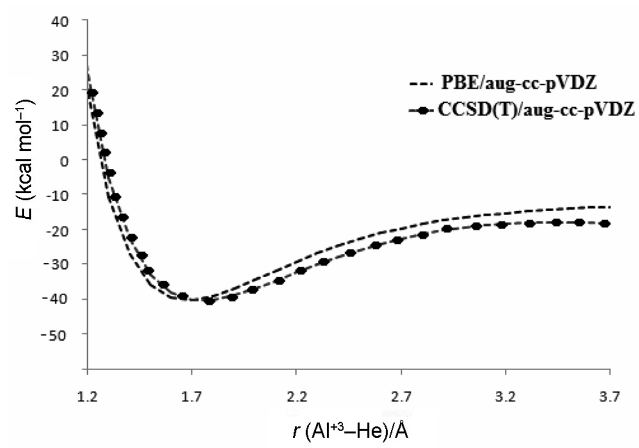

Figure 1. Potential energy curves for $AlHe^{3+}$ at CCSD(T) (line with bullet) and PBE (dotted line) using aug-cc-pVDZ level of theory.

Interestingly, the $N = 12$ structure is a true local minima while $N = 13$ is a second-order saddle point. This has also led us to interpret that the highest coordination number possible is 12. However, the incremental binding energy calculation reveals that the highest coordination number possible is not 12 but 11, as the binding energy for the addition of the 12th He atom to $AlHe_{11}^{3+}$ is negative.

We have calculated the incremental binding energy (E_{IB}) for each molecule using eq. (1) below, where E_b (N) is the binding energy of $AlHe_N^{3+}$ and E (He) is the total energy of He. We have calculated the E_{IB} values utilizing various density functional levels such as PBE[14], ωB97XD[15], PW91 (ref. 16) and wavefunction-based method MP2 (ref. 17) using aug-cc-pVDZ basis set. We have also calculated these values with the composite method CBS–QB3 for comparison (Table 2) because this method is widely used to obtain accurate energies of molecules. Figure 3 shows the E_{IB} values (kcal/mol) with increase in the value of N. It is evident from Table 2 and Figure 3 that E_{IB} values calculated using PBE and PW91 functionals are very close to the composite CBS–QB3 values

$$E_{IB} = -[E_b(N) - E_b(N-1) - E(\text{He})]. \quad (1)$$

The trend in E_{IB} values calculated at different levels of theory is similar. However, MP2 and ωB97XD values are lower than the composite CBS–QB3 values (Table 2). PBE and PW91 values are closer to the CBS–QB3 values. The E_{IB} values decrease gradually up to $N = 5$. Local maximum in the E_{IB} values is found for $N = 6$ and 8, indicating their structural stability. A steep decrease from $N = 6$ to 7 indicates disruption of the octahedron. Increase in E_{IB} value for $N = 8$ may be attributed to another stable structure. All these structures represent true local minimum in the potential energy surface. Interestingly, the icosahedral structure ($N = 12$) is also a local minimum;

Table 1. Minimum, maximum and average distances (Å) calculated at PBE/aug-cc-pVDZ level of theory

N	R_{min} (Al–He)	R_{max} (Al–He)	R_{av} (Al–He)	R_{av} (He–He)
1	1.746			
2	1.749	1.749	1.749	3.499
3	1.754	1.754	1.754	3.038
4	1.765	1.765	1.765	2.882
5	1.774	1.783	1.778	2.893
6	1.791	1.791	1.791	2.533
7	1.790	1.828	1.809	2.958
8	1.840	1.840	1.840	2.839
9	1.862	1.899	1.880	2.815
10	1.865	1.935	1.900	2.299
11	1.945	2.001	1.973	2.043
12	2.013	2.323	2.244	2.221

Table 2. Incremental binding energies (kcal mol^{-1}) of $AlHe_N^{3+}$ calculated at various levels of theory

N	PBE	ωB97XD	PW91	MP2	CBS–QB3
1	27.81	23.77	27.33	22.46	31.20
2	26.49	22.60	25.85	21.27	29.63
3	24.19	20.72	23.10	19.70	26.17
4	21.80	19.04	20.56	17.83	23.44
5	18.12	16.84	16.63	14.46	18.44
6	17.48	16.19	15.82	14.13	17.65
7	10.74	10.27	8.80	7.38	7.96
8	9.68	9.18	7.78	6.82	7.23
9	6.06	5.34	4.04	3.34	3.54
10	2.19	1.83	0.95	0.75	1.77
11	1.27	1.12	0.03	0.33	1.06
12	–0.56	–0.26	–3.99	–4.96	–6.08

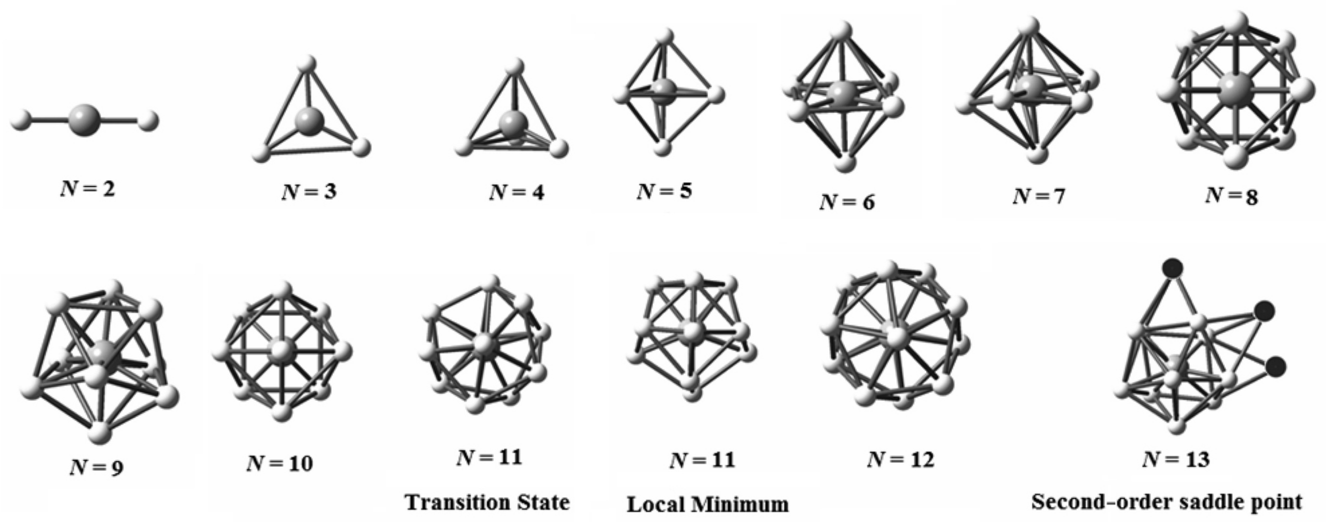

Figure 2. PBE/aug-cc-pVDZ optimized $AlHe_N^{3+}$ structures. The black He atoms in $N = 13$ structure denote atoms of the second shell.

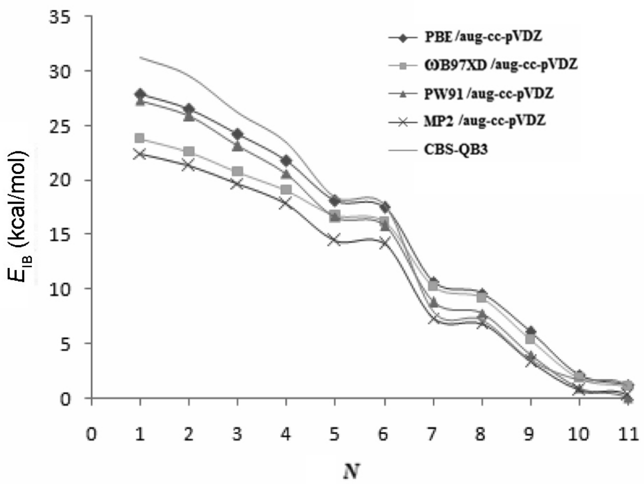

Figure 3. E_{IB} for $AlHe_N^{3+}$ ($N = 1$–11) calculated at various levels of theory.

Table 3. Incremental binding energies (kcal mol^{-1}) of $NaHe_N^+$ and $MgHe_N^{2+}$ clusters at PBE/aug-cc-pVDZ level of theory

N	$NaHe_N^+$	$MgHe_N^{2+}$
1	0.74	6.77
2	0.69	6.58
3	0.70	6.29
4	0.64	5.88
5	0.23	5.20
6	–0.23	4.97
7		3.17
8		3.08
9		3.08
10		0.55
11		0.28
12		–0.36

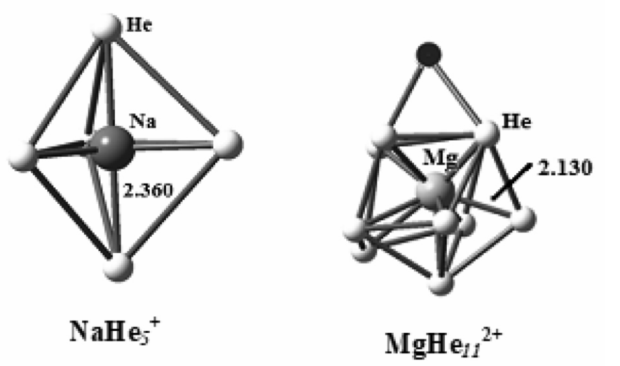

Figure 4. Optimized geometries of $NaHe_5^+$ and $MgHe_{11}^{2+}$ clusters. The black He atom denotes atom of the second shell.

however, the calculated E_{IB} value is negative (Table 2), which indicates that the limiting highest coordination number is 11.

We have calculated the binding energy of $NaHe_N^+$ and $MgHe_N^{2+}$ clusters to study the effect of charge on the stability of the complexes. Table 3 shows the binding energy data calculated at PBE/aug-cc-pVDZ level of theory. Figure 4 shows the optimized geometries for the highest values of N for which the binding energy is the lowest. The E_{IB} values for $NaHe_N^+$ clusters are very low and become negative at $N = 6$, while those for $MgHe_N^{2+}$ clusters are slightly higher and becomes negative at $N = 12$. Thus, for Mg^{2+}, the limiting coordination number is 11. It should be noted that the E_{IB} values for $AlHe_N^{3+}$ clusters are higher (Table 2) than those of $NaHe_N^+$ and $MgHe_N^+$ clusters. Even the binding energy of a He atom to neutral Al atom is very small (0.03 kcal mol^{-1}). This is in accordance with Jeff *et al.*[13] who showed that the interaction of neutral Al atom with He is almost negligible, and thus the

Al atom prefers to stay on the surface rather than moving to the interior of the He nanodroplets. Thus the binding energy values increase with increase in charge of the central metal, suggesting stronger interaction with charged species, which is also in accordance with Hermann *et al.*[4].

Further, the topological feature of the electron density of this interaction has been analysed within the realm of QTAIM[19]. Table 4 shows the QTAIM parameters. The average value of electron density at the Al–He bond critical points is very low. The Laplacian of electron density is positive and the average value of the local electronic energy density is very low. All these QTAIM parameters suggest closed-shell nature of this interaction.

Borocci *et al.*[21] have studied the bonding motif of noble gas compounds and suggested that local electronic energy density ($H(r)$ or, the opposite of Hamiltonian electron kinetic energy density) may provide information regarding the nature of non-covalent interaction. $H(r)$ is positive for all the cases. A positive value of $\nabla^2\rho$ (av) and $H(r)$ clearly indicates the closed shell (or non-covalent) nature of this interaction. The average electron density at the Al–He bond critical point is found to correlate well with the average Al–He distance and E_{IB} values (Figure 5).

In conclusion, the present study revealed that the limiting highest coordination number possible for AlHe_N^{3+} is 11, which is also supported by incremental binding energy calculations. This structure contains all the 11 He atoms in one shell and the stability of this species suggests that this can be identified by mass spectroscopic methods. The versatility of He has triggered Hermann *et al.*[4] and Kaltsoyannis[2] to speculate coordination number of 15 and 17 for Pb^{2+} and Ac^{3+} respectively. It may be noted that these two ions have larger radii compared to Al^{3+} (ref. 22). To the best of our knowledge, this is the highest coordination number ever reported, especially for a small Al^{3+} ion having a radius of only 0.53 Å (ref. 22).

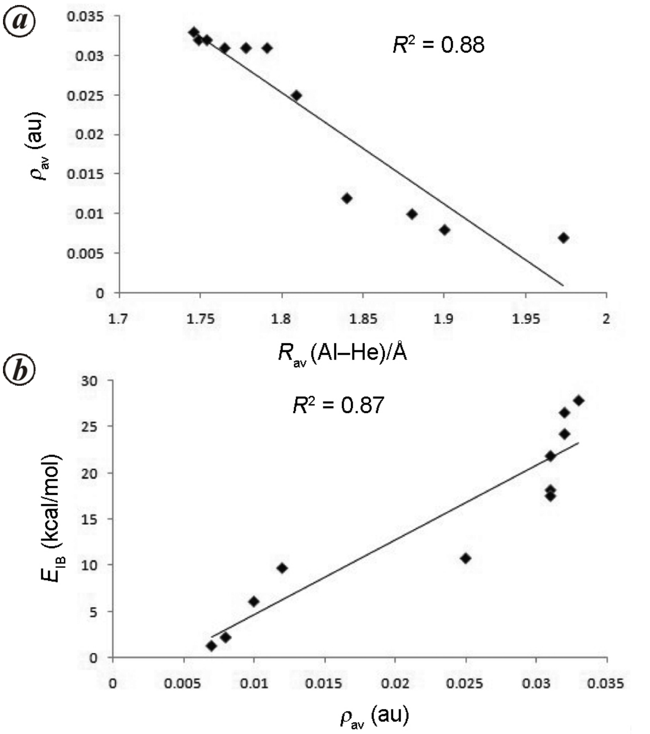

Figure 5. Correlation plot between (***a***) average electron density (ρ_{av}) at the Al–He bond critical point and average Al–He distance [R_{av} (Al–He)], and (***b***) incremental binding energy (E_{IB}) and average electron density (ρ_{av}) at the Al–He bond critical point.

Table 4. Average values of electron density at the bond critical point (ρ), Laplacian of electron density ($\nabla^2\rho$) and local electronic energy density, $H(r)$ calculated at PBE/aug-cc-pVDZ level of theory. All values are in au

N	ρ(av)	$\nabla^2\rho$ (av)	$H(r)$ (av)
1	0.033	0.264	0.132
2	0.032	0.259	0.013
3	0.032	0.255	0.012
4	0.031	0.244	0.012
5	0.031	0.234	0.011
6	0.031	0.225	0.011
7	0.025	0.169	0.010
8	0.012	0.022	0.009
9	0.010	0.021	0.008
10	0.008	0.019	0.006
11	0.007	0.006	0.005

1. Miao, M., Helium chemistry: react with nobility. *Nature Chem.*, 2017, **9**, 409–410.
2. Kaltsoyannis, N., Seventeen-coordinate actinide helium complexes, *Angew. Chem. Int. Ed.*, 2017, **56**, 7066–7069.
3. Sloane, N. J. A. and Conway, J. H., Sphere Packings, Lattices and Groups, Springer, New York, 1999.
4. Hermann, A., Lein, M., and Schwerdtfeger, P., The search for the species with the highest coordination number. *Angew. Chem. Int. Ed.*, 2007, **46**, 2444–2447.
5. Frank, F. C. and Kasper, J. S., Complex alloy structures regarded as sphere Ppackings. I. Definitions and basic principles. *Acta Crystallogr.*, 1958, **11**, 184–190.
6. Bichara, C., Pellegatti, A. and Gaspard, J.-P., Properties of liquid group V elements: a numerical tight binding simulation. *Phys. Rev. B*, 1993, **47**, 5002–5007.
7. Johnston, R. L., *Atomic and Molecular Clusters*, Francis, London, 2002.
8. Komura, Y. and Tokunaga, K., Structural studies of stacking variants in Mg-base Friauf–Laves phases. *Acta Crystallogr. Sect. B*, 1980, **36**, 1548–1554.
9. Dong, X. *et al.*, React with nobility. *Nature Chem.*, 2017, **9**, 440–445.
10. Liu, H., Yao, Y., and Klug, D. D., Stable structures of He and H_2O at high pressure. *Phys. Rev. B*, 2015, **91**, 014102-7.
11. Hotokka, M., Kindstedt, T., Pyykkö. P. and Roos, B., On bonding in transition-metal helide ions. *Mol. Phys.*, 1984, **52**, 23–32.
12. Reho, J. H., Merker, U., Radcliff, M. R., Lehmann, K. K. and Scoles, G., Spectroscopy and dynamics of Al atoms solvated in superfluid helium nanodroplets. *J. Phys. Chem. A*, 2000, **104**, 3620–3626.
13. Jeff, J. *et al.*, Metastable aluminium atoms floating on the surface of helium nanodroplets. *Phys. Rev. Lett.*, 2015, **114**, 233401.

14. Perdew, J. P., Burke, K. and Ernzerhof, M., Generalized gradient approximation made simple. *Phys. Rev. Lett.*, 1996, **77**, 3865–3868.
15. Chai, J.-D., and Head-Gordon, M., Long-range corrected hybrid density functionals with damped atom–atom dispersion corrections. *Phys. Chem. Chem. Phys.*, 2008, **10**, 6615–6620.
16. Perdew, J. P., in *Electronic Structure of Solids* 1991 (ed. Ziesche, P. and Eschrig, H.), Akademie Verlag, Berlin, 1991, 11; Perdew, J. P., Chevary, J. A., Vosko, S. H., Jackson, K. A., Pederson, M. R., Singh, D. J. and Fiolhais, C., Atoms, molecules, solids, and surfaces: applications of the generalized gradient approximation for exchange and correlation. *Phys. Rev. B*, 1992, **46**, 6671–6687; Perdew, J. P. *et al.*, Erratum: atoms, molecules, solids, and surfaces – applications of the generalized gradient approximation for exchange and correlation. *Phys. Rev. B*, 1993, **48**, 4978.
17. Møller, C. and Plesset, M. S., Note on an approximation treatment for many-electron systems. *Phys. Rev.*, 1934, **46**, 618–622; Binkley, J. S. and Pople, J. A., Møller-Plesset theory for atomic ground state energies. *Int. J. Quantum Chem.*, 1975, **9S**, 229–236; HeadGordon, M., Pople, J. A. and Frisch, M. J., MP2 energy evaluation by direct methods. *Chem. Phys. Lett.*, 1998, **153**, 503–506.
18. Frisch, M. J. *et al.*, Gaussian 16, Revision A.03, Gaussian, Inc, Wallingford CT, USA, 2016.
19. Bader, R. F. W., *Atoms in Molecules: A Quantum Theory*, Oxford University Press, Oxford, UK, 1990; Bader, R. F. W., A quantum theory of molecular structure and its applications. *Chem. Rev.*, 1991, **91**, 893–928.
20. Tian, L., Multiwfn: a multifunctional wavefunction analyser (version 3.1), 2015; http://Multiwfn.codeplex.com; accessed on 22 May 2015).
21. Borocci, S., Giordani, M. and Grandinetti, F., Bonding motifs of noble–gas compounds as described by the local electron energy density. *J. Phys. Chem. A*, 2015, **119**, 6528–6541 and references therein.
22. Shannon, R. D., *Acta Crystallogr. Sect. A*, 1976, **32**, 751.

ACKNOWLEDGEMENTS. A.K.G. thanks the Science and Engineering Research Board (SERB), Government of India for providing financial assistance through a project (project no. ECR/2016/001466).

Received 6 November 2017; revised accepted 6 February 2018

doi: 10.18520/cs/v114/i10/2138-2142

'*Prosopis* for prosperity': using an invasive non-native shrub to benefit rural livelihoods in India

Debbie Bartlett[1,*], Sarah Milliken[2] and Dayesh Parmar[3]

[1]Faculty of Engineering and Science, University of Greenwich, Central Avenue, Chatham Maritime, Medway, Kent ME4 4TB, UK
[2]Department of Architecture and Landscape, University of Greenwich, Park Row, Greenwich, London SE10 9LS, UK
[3]Gujarat Institute of Desert Ecology, Bhuj 370 040, India

Prosopis juliflora **is an invasive non-native shrub species which has an adverse impact on natural habitats in many parts of India, with detrimental effects on both wildlife and traditional livestock-based economies. Attempts to eradicate this very adaptable and resilient species tend to be unsuccessful and expensive. Here we report on two management techniques that could be used not only to minimize its ecological impact, but also to acknowledge its value as a resource to support rural livelihoods: biochar production and the creation of stock-proof living fences.**

Keywords: Biochar, living fence, *Prosopis juliflora*, rural livelihoods.

THIS study was undertaken in response to the need for soil improvement and stock-proof fencing that emerged during a participatory ecosystem services assessment of the coastal plain of Kachchh district, Gujarat, India[1,2]. The project, funded by the British Council UK–India Education and Research Initiative (UKIERI), was initiated due to concern about the spread of *Prosopis juliflora* and its impact on native plant species, particularly in the grasslands which are highly valued for wildlife and are a traditional grazing resource[3]. *P. juliflora* is native to South America and was introduced to Kachchh in the 1960s to prevent the Rann desert from encroaching onto the Banni grassland, an important area for grazing and biodiversity. Remote sensing data show that the shrub has spread at a rate of about 25 km^2/yr, and it is predicted that by 2020 more than 56% of the grassland will be under *P. juliflora*[4]. The species has colonized the arid Kachchh landscape so successfully that ecologists are now recommending that steps should be taken to eradicate it. In some areas it has replaced native species such as *Prosopis cineraria* and gugal (*Commiphora wightii*), which are important sources of medicine for local people[5]. The invasion of pastureland by *P. juliflora* threatens traditional livestock-based economies: the thorny shrubs restrict access to water, and can cause injury to the animals. While the pods can be used as a high protein feed for goats, sheep and camels, the high sugar content makes them indigestible for buffalo and cattle[6].

*For correspondence. (e-mail: D.Bartlett@greenwich.ac.uk)